8 August 2024
maruya@hep.phys.titech.ac.jp

CERN Summer Student Program Report

Yasuhiro Maruya [1]
Supervisor: Tomohiro Inada, Susanne Kühn

Keywords: CERN summer student programme, FASER, electron neutrino, Likelihood

Summary

Measuring the flux of neutrino from the proton-proton collision at the Large Hadron Collider connects to further understanding of the QCD interaction at p-p collision. FASER experiment aims to measure the neutrino flux and already detected the neutrinos from p-p collision. In this report, we study a new way to detect electron neutrino using the FASER detector. Our new way aims to detect electron neutrino interactions in the electromagnetic calorimeter of the FASER detector. Using the Monte Carlo simulation, we evaluate the possibility of detecting electron neutrino by our method and the possibility of measuring its cross-section. The statistical analysis indicated that, while the current significance for detecting ν_e is not reached to 3σ, we will able to detect ν_e using this method by the end of Run-4. The significance becomes 5σ at about 450 fb^{-1} without the muon detector, at about 250 fb^{-1} with the muon detector behind the calorimeter with sufficient materials. The uncertainty of cross-section becomes under 70 % at 500 fb^{-1}. Additionally, the inclusion of the muon detector behind the calorimeter could reduce the uncertainty of measuring about 10 %.

Contents

[1]Department of Physics, Tokyo Institute of Technology, Tokyo, Japan

1 Introduction

This report is part of the CERN Summer Student Programme 2024. During this programme, I participated in the FASER experiment [9] and conducted research on evaluating the possibility of detecting ν_e and measuring its cross-section using the FASER detector.

2 ForwArd Serch ExpeRiment (FASER)

2.1 Physics of the FASER experiment

There are two main purposes of the FASER experiment. The first one is searching for BSM long-lived neutral particles. The Standard Model is consistent with most experimental results. However, it is believed that there are undiscovered particles that could resolve some unsolved problems of the Standard Model. The FASER experiment is searching for these particles [4, 1]. The second purpose is to measure the neutrino flux from proton-proton collisions in the LHC (Large Hadron Collider). The measurement of neutrino flux provides further insights into Quantum Chromo Dynamics (QCD) interactions, such as D meson fragmentation, charm production, and Nuclear Parton Distribution Functions (PDFs).

2.2 FASER detector

The detector for the FASER experiment is located 480 m downstream from the ATLAS interaction point. The FASER detector consists of scintillators, permanent magnets, trackers, electromagnetic calorimeters, and the FASER ν emulsion detector.

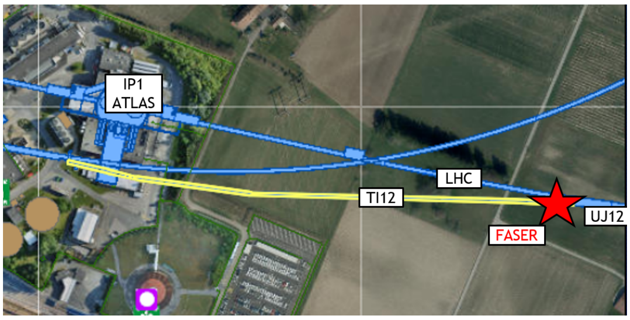

Figure 1: Location of FASER Detector [5]

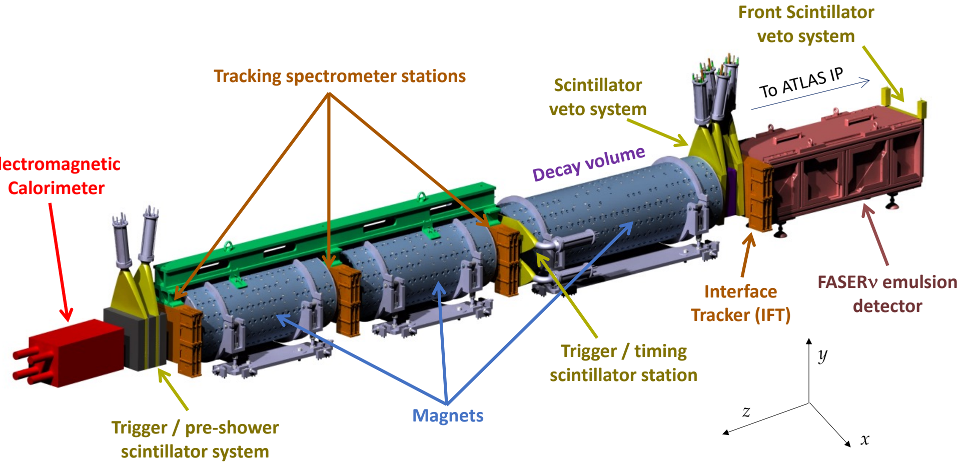

Figure 2: Schematic of the FASER Detector[5]

2.3 HL-LHC

LHC is going to be update after the current run (Run 3) ends.
In the next run (Run4), the peak luminosity becomes higher than now. The plan of the HL-LHC is summarized[10].
The integrated luminosity of Run4 will be more than 500 fb^{-1}.

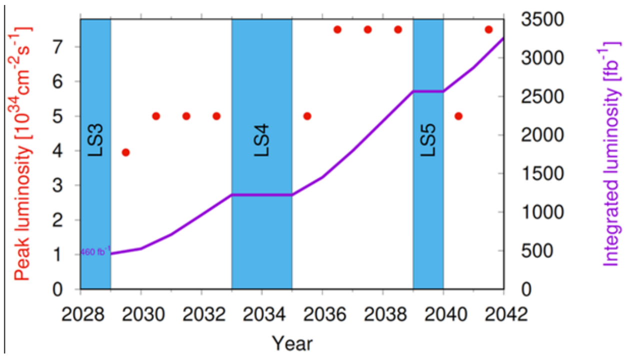

Figure 3: Plan of HL-LHC[10]

3 Analysis to detect ν_e only using FASER detector

3.1 Motivation

The first direct detection of collider ν_μ was performed by the FASER detector [3]. Additionally, the first measurement of collider ν_e and ν_μ interaction cross-sections was conducted by the FASER ν emulsion detector [2]. However, due to increased luminosity, the FASER collaboration plans not to use the FASERν emulsion detector in HL-LHC. Thus, detecting collider ν_e using only the FASER electronic detector is necessary.

3.2 Procedure to detect ν_e

I came up with two methods to detect ν_e using only the electric detector of the FASER.

3.2.1 ν_e interacts in the veto system

The first method aims to detect ν_e interactions in the lead absorber which is located in the veto system. By requesting tracks in tracker stations 1, 2, and 3 and selecting events where the calorimeter energy deposits do not correspond to muon ionization, ν_e can be identified. However, the number of signal events is insufficient for cross-section measurement, and there are significant ν_μ backgrounds. Thus, this method is not worth considering at this time.

3.2.2 ν_e interacts in the pre-shower and calorimeter system

The second one aims to detect ν_e interactions in the absorber in the pre-shower system and Electromagnetic calorimeter. ν_e charged current interaction produces the electron and makes an electromagnetic shower in the calorimeter, and other particles produced in neutrino interaction don't make an EM shower except for neutral meson.

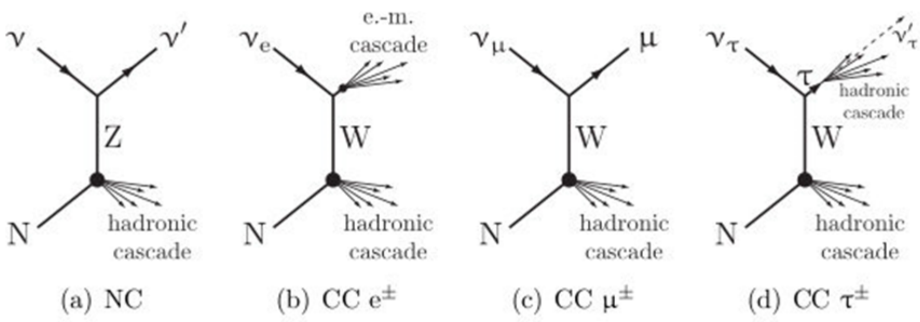

Figure 4: Classification of neutrino interaction [6]

Thus, ν_e makes higher energy deposits to the EM calorimeter than any other interaction. This feature is most important when dividing signal charged current ν_e interaction and other background interactions.
The number of neutrino interactions has been estimated as a background in ALPs search[1]. It is sufficient to detect, so I concentrated on this analysis.

3.3 Monte Carlo Simulation

It is the same as the background event sample in the ALPs search[1].

3.4 Selection

Event selection is the following

1. Selecting events with calorimeter triggers, the Calorimeter trigger is done when the energy deposit is above 20 GeV. (data only.)
2. Calorimeter timing is consistent with the bunch crossing timing. (> -5 ns and < 10 ns). (data only.)
3. Veto/VetoNu scintillator corresponds to no signal ($<$ 0.5 MIPs).
4. Timing Scintillator charge corresponds to no signal ($<$ 0.5 MIPs).
5. The number of cluster in the tracker station 3 is under 10. Please see 3.5.1.
6. Calorimeter energy $E_{calo} > 150$ GeV [1]. The threshold should be optimized to reduce the Neutral Hadron Background and to gain the significance of the detection. See the section 3.5.3 and 3.9. Now, the threshold is set to 150 GeV.

Figure 5 shows the distribution of calibrated calorimeter energy under the selection above.[2] The background contamination of other neutrino interactions is 63 % at $E_{calo} >$ 150 GeV, and 43 % at $E_{calo} > 500$ GeV. Figure 6 show the background ration under the events over $E_{calo,cut}$. The trend follows that the electron neutrino tends to deposit higher energy.

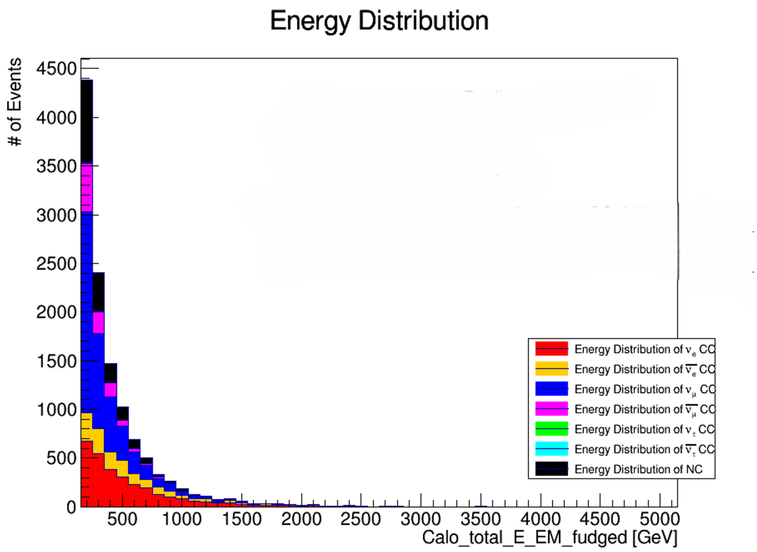

Figure 5: Calibrated calorimeter energy distribution at 10 ab^{-1}

[1] E_{calo} = Calo total E EM fudged. It is calibrated

[2] For internal, This is obtained by MC simulation(MC24, 20025,20026,20035,10 ab^{-1})

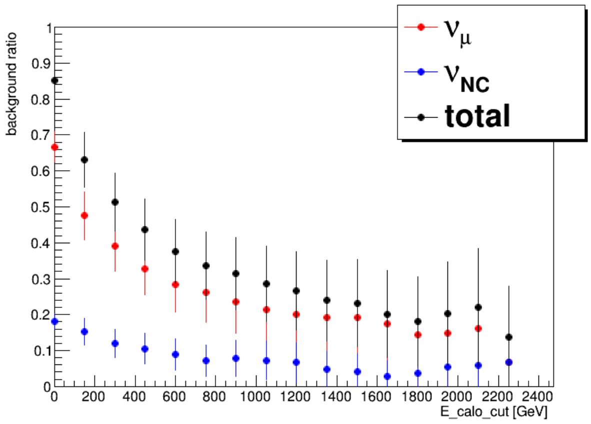

Figure 6: Background ratio of the events over $E_{calo,cut}$. The statistical error bar is plotted.

3.5 Background events

The background events for charged current ν_e detection can be classified as follows:

3.5.1 Interaction occurring in the magnet

The event where ν_e interacts in the magnet can make high-energy deposits to the calorimeter.

The structure of the magnet and its magnet fields in the MC simulation is not clear to me and its reality has never been evaluated, so to reduce the procedure to evaluate the systematic uncertainty of this simulation, I set these events as background.

When we open the data, we should evaluate which is bigger, the statistical effect of using this magnet event or the systematic uncertainty of MC simulation.

However, a tracker station exists between the magnet and the pre-shower system. Thus, using the hit information of the tracker station 3, it is rejected and becomes negligible.

Figure7 shows the distribution of the number of clusters in the tracker station 3 of the signal events. The number of clusters is the number of hits in the Si strip detector. The number of clusters of the event where the ν_e interacts in the magnet is bigger than other places.

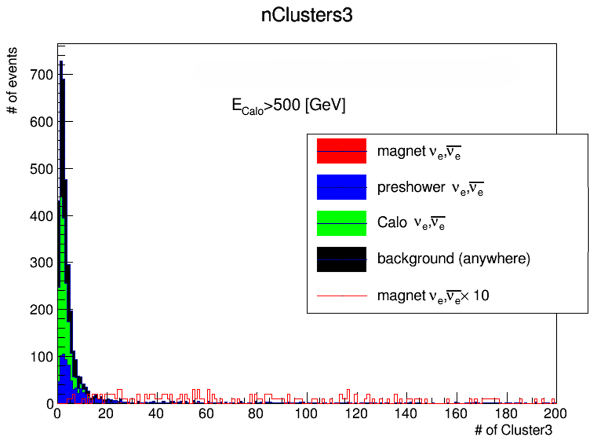

Figure 7: Distribution of the number of Clusters in the tracker station 3 of signal events. The color shows the place where interaction occurs.

Thus, the selection is set to the number of clusters at the tracker station 3: nCluster3 $<$ 10, then the magnet event is rejected except for 4 events at 10 ab^{-1}. Thus, this background becomes negligible.

3.5.2 Other neutrino interaction

There are two main background neutrino interactions. The number of charged current ν_τ interactions is negligible. The first one is the CC ν_μ interaction. The second one is the NC interaction. I have an idea to use pre-shower scintillator charge information to distinguish the NC interaction events and signal events. However, the result shows it is not easy.
When CC ν_μ interaction occurs in the pre-shower or the calorimeter system, the produced muon always passes through the calorimeter. As a suggestion for the FASER Run4 detector, I investigated the rejection rate of background events and signal events if there is sufficient shielding and muon veto scintillator behind the calorimeter. However, performing an MC simulation with a new scintillator is not cost-effective, so I use the truth information with no shielding materials,
The setting of the scintillator is the following;

1. Located at $z = 5600$ mm; about 2400 mm behind the calorimter.
2. Square scintillator, its size is 600 mm $\times$ 600 mm, and its center match to the center of the FASER detector.

To use the truth information with no shielding materials, there are some assumptions following;

1. If muon produced in the calorimeter and the pre-shower system reaches the muon veto Scintillator, I assume a 99.7 % probability of exclusion.
2. Hadron shower is completely shielded.

Under this assumption, calorimeter energy distribution becomes Figure 8 and the rejection ratio is summarized in table 1. Most of the background CC ν_μ events are rejected, but some of the signal is also rejected. There are still the NC backgrounds.

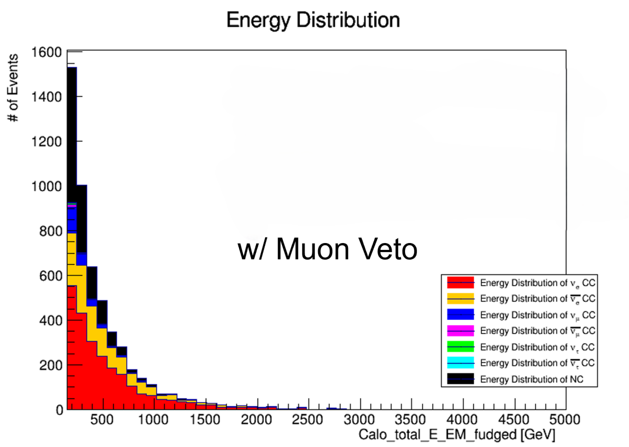

Figure 8: Calibrated calorimeter energy distribution at 10 ab^{-1} with muon veto scintillator.

events	Rejection ratio @ $E_{calo} > 150$ GeV
Signal (CC ν_e)	0.20
CC ν_μ	0.95
NC	0.28
Total background	0.79

Table 1: Rejection ratio with muon veto scintillator

3.5.3 Backgrounds from other sources

Large angle muons

Muons traversing the detector at a large angle may miss the veto scintillator and trigger system, interact, and make high-energy deposits to the calorimeter.
MC samples have been produced of muons traversing FASER using FLUKA. There are no background events that pass the selection. The background is highly rejected by requesting no deposit to the Veto system and the trigger system, and $E_{calo} > 20$ GeV.

Neutral Hadron

Neutral hadron produced by muon interaction in the rock in front of FASER detector may become the background. Most of these particles decay in the emulsion detector.
There are no dedicated MC samples, so estimating this background is not easy and we must do it by data-driven. In [1] and [3], the number of background is estimated. In that analysis, The background with $E_{calo} > 500$ GeV is estimated as negligible.
Our selection criterion of E_{calo} should be set to suppress this background. However, I don't

open the data, so I neglect the background events in this study, and just set the selection $E_{calo} > 150$ GeV.

Non-Collision

The particles from Non-collision sources may become background.
The criteria are the same as ALPs search [1], and the background from Non-Collision is estimated as negligible. Thus, in this analysis, the Non-Collision background is negligible.

Veto System Inefficiency

Inefficiencies of the five veto scintillators and trigger system may cause muon to pass the selection.
The criteria are the same as ALPs search [1], and the background is estimated as negligible. Thus, in this analysis, the background of the Veto System Inefficiency is negligible.

3.6 Systematic uncertainty

Systematic uncertainties arise from some sources and affect both expected signal yields and background estimates.

1. Calorimeter energy scale:
   In the Dark photon search [2], it was estimated by comparing the peak position of E/p between the MC simulation and test beam. We should use the same systematic uncertainty 6 %.
   However, the way to consider the systematic uncertainty of the calorimeter energy scale is just developing, so we neglect this systematic uncertainty currently.

2. Integrated Luminosity:
   This uncertainty is provided by the ATLAS collaboration. It was 2.2% in 2022 data. Considering the same uncertainty as far.

3. Number of clusters in the tracker station 3:
   This systematic uncertainty arises from the difference between MC simulation and Real detector. Now I assume it is negligible.

4. Neutrino flux estimation:
   Due to the undefined things in QCD interaction in the p-p collision, we can't expect the neutrino flux accurate. This systematic uncertainty from flux estimation is discussed in [7]. Following this.
   In this method, the systematic uncertainty of the cross-section is not contained.

5. Neutrino cross-section expectation uncertainty at the generator:
   This systematic uncertainty from the generator is discussed in [7]. Neutrino flux estimation and cross-section uncertainty will be discussed in Section 3.7.2.

6. Hadronization in MC simulation:
This systematic uncertainty arises in the Geant4 simulation. We should check the difference between "Physiclist" by comparing the results.
However, the derivation process has not been done yet. So, we neglect this systematic uncertainty. This uncertainty is smaller than one of the flux estimation.

7. Reality of structure in the MC simulation:
As I said in section 3.5.1, we have to consider the systematic uncertainty of the reality of the MC simulation. However, currently, I assume the structure of the calorimeter and the pre-shower system is reliable. The structure of the magnet and its magnet fields are not reliable, but we reject the event in which interaction occurs in the magnet, so there is no need to consider the systematic uncertainty from the magnet structure.

3.7 Statistical Analysis

To evaluate the possibility of detecting ν_e, I calculated the significance of the signal detection using binned likelihood methods to the calorimeter energy distribution with assumption that the data follow the MC simulation.
To evaluate the possibility of measuring the cross-section of ν_e, I calculated the uncertainty of the cross-section using binned likelihood methods to the calorimeter energy distribution with assumption that the data follow the MC simulation.

3.7.1 parameterized binned Likelihood method

To measure the cross section per energy, we have to set the parameter depending on neutrino energy E_{truth}. The density function of signal events on E_{truth} are proportional to cross-section $\sigma(E_{truth})$ times differential flux $\phi(E_{truth})$. So setting the coefficient parameter at each bin on E_{truth} to the density function, we can measure the cross-section times flux. The method is systematized as follows:

1. Getting the 2D plot E_{calo} vs E_{truth}(Figure 9) from MC simulation.
2. Binning the E_{calo} and E_{truth} to i and j.
3. Estimating the number of event $n^{MC}(i,j)$ at the target luminosity by scaling
4. Calculating the statistical uncertainty and systematic uncertainty on $n^{MC}(i,j)$.
5. Parameterize the estimated value as follows:[3]

$$n^{MC}_{para}(i,j) = \alpha_j \times n^{MC}(i,j) \propto \alpha_j < \sigma_{\text{theory}} \times \phi_{\text{MC}} >_j$$

6. Set the likelihood function and fit to data.
7. Post-fit α parameter value means as follows:

$$\alpha_j = \frac{< \sigma \times \phi >_i}{< \sigma_{\text{theory}} \times \phi_{\text{MC}} >_j}$$

[3] $<>_j$ mean the average in j bin.

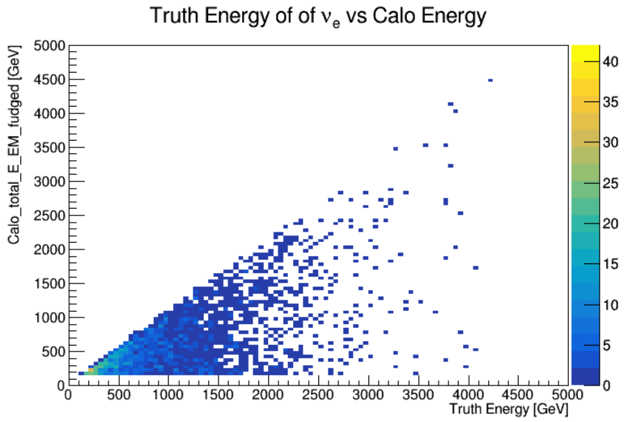

Figure 9: 2D distribution of ν_e,$\bar{\nu_e}$on E_{truth}, E_{calo}. This distribution was obtained under the selection without the muon veto detector

The Likelihood function L is set as follows;

$$L(\boldsymbol{n_{data}}|\boldsymbol{\alpha}, \nu_{\text{bkg}}, \boldsymbol{\nu_{sys}}, \boldsymbol{\gamma}) = \prod_{i}^{N} \left[\text{Pois}(n^{i}_{\text{data}}|n^{exp}_{i}) \times \text{Pois}(m_i|\gamma_i m_i)\right] \times f_{sys}(\nu_{sys}) \quad (1)$$

$$n^{exp}_{i} = \sum_{j}^{M} \left[\alpha_j \gamma_i \prod_{sys} [\eta^{j}_{sys,i}(\nu_{sys})] \times n^{MC}(i,j)\right] + \nu_{\text{bkg}} \gamma_i \prod_{sys} [\eta^{\text{bkg}}_{sys,i}(\nu_{sys})] \times n^{MC}_{\text{bkg}}(i) \quad (2)$$

- i - the bin number of E_{calo}.
- N - the total number of E_{calo} bin.
- j - the bin number of E_{truth} .
- M - the total number of E_{truth} bin.
- $\boldsymbol{n_{\text{data}}} = \{n^{i}_{\text{data}}|i \in 0 \sim N\}$ - The number of observed events at each bin on E_{calo}.
- $\boldsymbol{\alpha} = \{\alpha_j|j \in 0 \sim M\}$ - Coefficient parameter at each bin on E_{truth}.
- ν_{bkg} - Normalization factor of the background events.
- $\boldsymbol{\nu_{sys}} = \{\nu_{sys}|sys \in \{\text{Flux}, \text{Luminocity}\}\}$
  - Nuisance parameter for each systematic uncertainty.
- $\gamma = \{\gamma_j|j \in 0 \sim M\}$ - Scale factor used for Monte Carlo statistical uncertainties. Followed [8].
- m_i - the number of total events at MC simulation data (before scaling) at each bin.[4]

[4]However, in [8] m_b is inverted. This is not correct. $m_b = \tau_b$ is the number of total events at MC simulation data (before scaling) at each bin.https://root-forum.cern.ch/t/beeston-barlow-light-math-in-histfactory-manual/47901

- $f_{sys}(\nu_{sys})$ - the constraint term for systematic uncertainty. In this analysis,

$$f_{sys}(\nu_{sys}) = \text{Gaus}(a = 0|\nu_{sys}, \sigma = 1)$$

- $\eta^{j(\text{bkg})}_{sys,i}(\nu_{sys})$ - Interpolation/ extrapolation terms of systematic uncertainty with nuisance parameters. For luminosity uncertainty, it is Piecewise Exponential[8]. For others, it is Piecewise Linear[8].[5]

3.7.2 Flux model systematic uncertainties and cross-section uncertainty

Using the above methods, we can measure the cross-section times flux. To measure the cross-section, the systematic uncertainty from the flux expectation does not need to be considered if there is no binning.
However, we are doing the binning, so we must consider the difference between the flux model in one E_{truth} bin region.
Also, we must consider the systematic uncertainty of cross-section in one bin region. The systematic uncertainty arises at the generator. However, the uncertainty between the cross-section is estimated under 6 %[7] at 100 GeV $\sim$ 3 TeV. The uncertainty is less than one of the flux model, so we assume it is negligible now.
The methods evaluating the systematic uncertainty is follow the ALPs search [1] and [7].
The model of p-p collision is done by each production method. Sibyll, Epos, QGSJET, and Pythia simulate the pion and kaon production. Monash simulates the charm hadron production and it has a maximum production simulation and minimum production simulation. Thus I set the systematic uncertainty as follows

1. $n^j_{i,\pm 1\sigma_{Flux}}$: The scaled number of events by the model which expects the highest (lowest) amount.

2. n^j_i: The scaled number of events by EPOS and Monash model.

Figure 10 shows the distribution of n^j_i of each model. In this Figure, The bin on E_{truth} is set to $0, 800, 1300, 5150$ GeV.

[5] In [8], Luminosity systematic uncertainty isn't treated as "OverallSys". I set the Luminosity systematic uncertainty as "OverallSys" by the default of TRExFitter. And others are treated as "HistoSys"

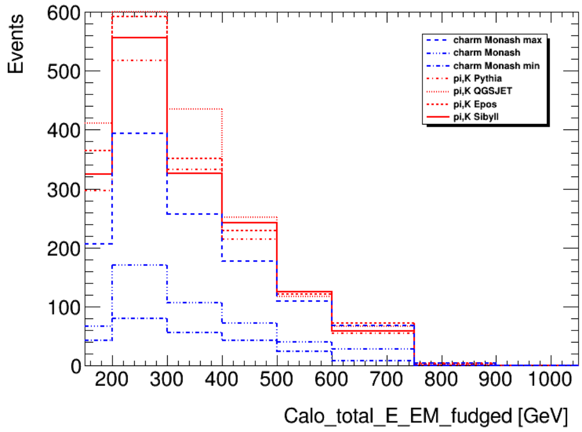

(a) signal bin 0: E_{truth}[0,800] GeV

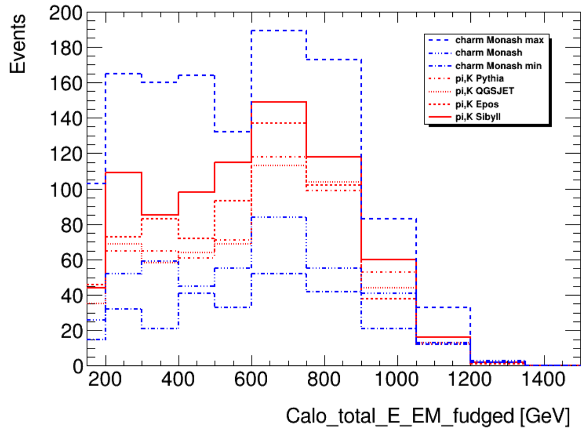

(b) signal bin 1: E_{truth}[800,1300] GeV

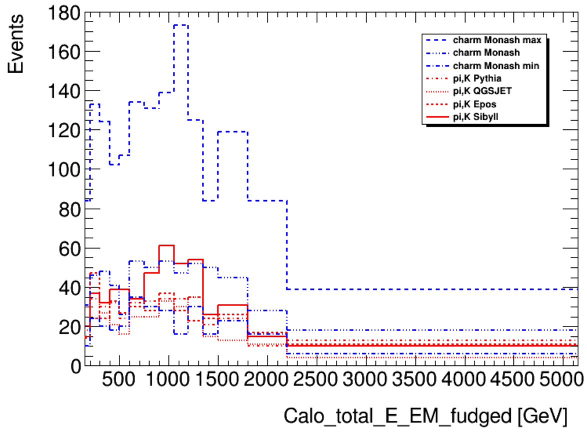

(c) signal bin 2: E_{truth}[1300,5150] GeV

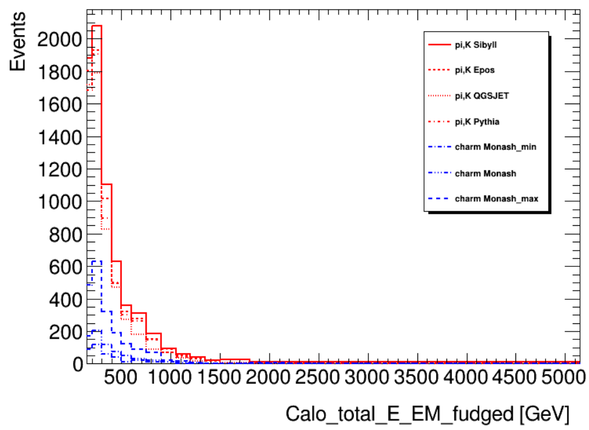

(d) background

Figure 10: Distribution of n_i^j of each model at 10 ab^{-1} without the muon veto detector. In this Figure, The bin on E_{truth} is set to $0, 800, 1300, 5150$ GeV.

On the other hand, we can select the best model to explain the pp-collision. This is discussed in the section 3.10.

3.7.3 significance calculation

To get the significance of the detection, there is a need to integrate the α to scale factor of signal events ν_{sig}. When calculating the significance, the Likelihood function is set as follows:

$$L(\boldsymbol{n_{data}}|\nu_{\text{sig}}, \nu_{\text{bkg}}, \boldsymbol{\nu_{sys}}, \boldsymbol{\gamma}) = \prod_i^N \left[\text{Pois}(n^i_{\text{data}}|n_i^{exp}) \times \text{Pois}(m_i|\gamma_i m_i)\right] \times f_{sys}(\nu_{sys}) \tag{3}$$

$$n_i^{exp} = \nu_{\text{sig}}\gamma_i \prod_{sys}[\eta^{\text{sig}}_{sys,i}(\nu_{sys})] \times n^{MC}(i) + \nu_{\text{bkg}}\gamma_i \prod_{sys}[\eta^{\text{bkg}}_{sys,i}(\nu_{sys})] \times n^{MC}_{\text{bkg}}(i) \tag{4}$$

$$n^{MC}(i) = \sum_j^M n^{MC}(i,j) \tag{5}$$

3.8 Results from the Asimov data

Likelihood fit is performed on the Asimov dataset. The Asimov dataset is a dataset that completely follows the MC simulation. Using this method, we can evaluate the possibility without real data.

The bin on E_{truth} is set to $0, 800, 1300, 5150$ GeV. So, there are three alpha parameters.

Figure 11,12 shows the dependence of the significance on the luminosity. Figure 13,14 shows the dependence of the uncertainty of the α parameter on the luminosity.

The significance becomes 5σ at about 500 fb^{-1} whether there is a muon detector or not. The difference between with or without the muon detector doesn't appear in the significance growth curve with systematic uncertainty.

In Figure 13, the uncertainty drops as the luminosity becomes big.

Figure 16 shows the squared uncertainty of α at each bin. In Figure 16, you can see the statistical uncertainty significantly decrease as the luminosity becomes big, but Flux uncertainty is not so.

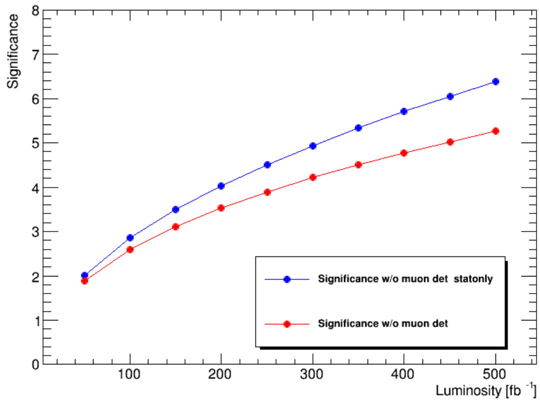

Figure 11: Growth curve of the significance without the muon veto detector. We only consider the flux model uncertainty and luminosity uncertainty. The red one is the result considering systematic uncertainty. The blue one is the result of not considering systematic uncertainty.

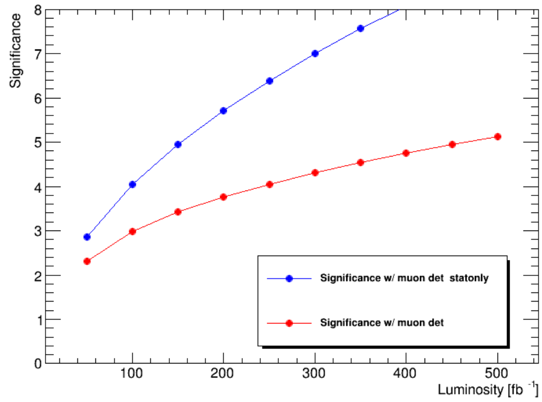

Figure 12: Growth curve of the significance with the muon veto detector. We only consider the flux model uncertainty and luminosity uncertainty. The red one is the result considering systematic uncertainty. The blue one is the result of not considering systematic uncertainty. The overflow is from the bug of the TRExFitter.

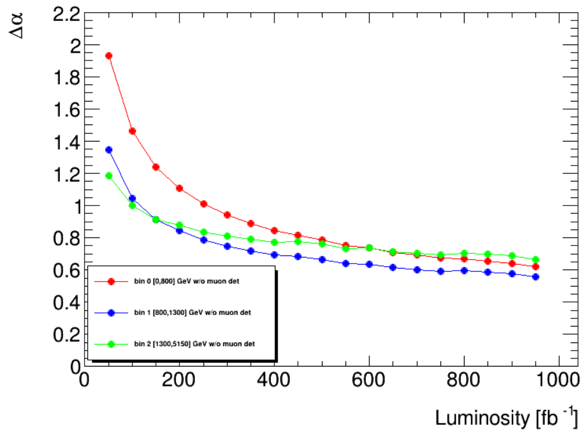

Figure 13: Growth curve of the uncertainty of the α parameter without the muon veto detector. We only consider the flux model uncertainty and luminosity uncertainty.

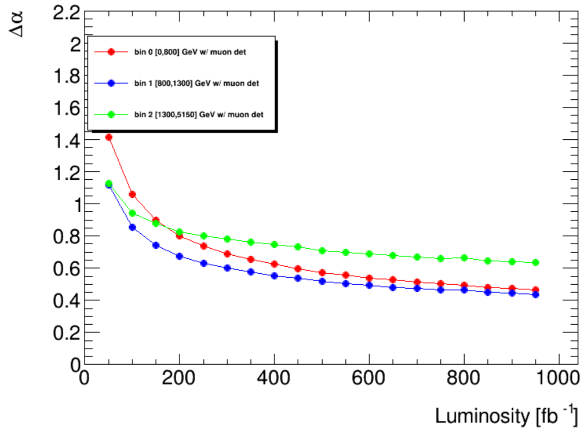

Figure 14: Growth curve of the uncertainty of the α parameter with the muon veto detector. We only consider the flux model uncertainty and luminosity uncertainty.

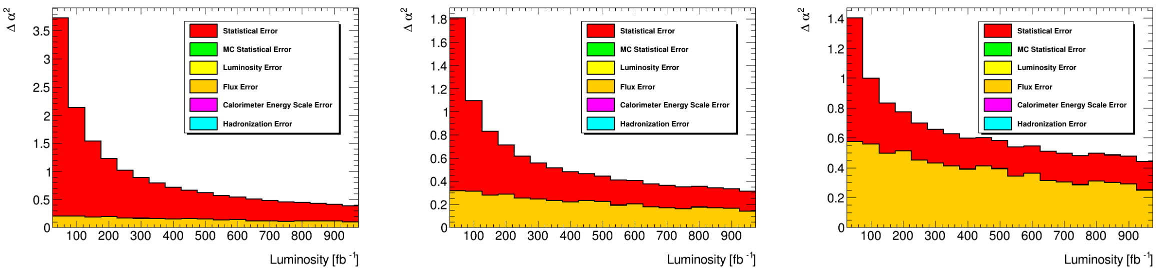

(a) bin 0: [0,800] GeV (b) bin 1: [800,1300] GeV (c) bin 2: [1300,5150] GeV

Figure 15: square of the α uncertainty of each bin. Stacked. The calorimeter uncertainty and Hadronization uncertainty are in the legend, but we don't calculate them.

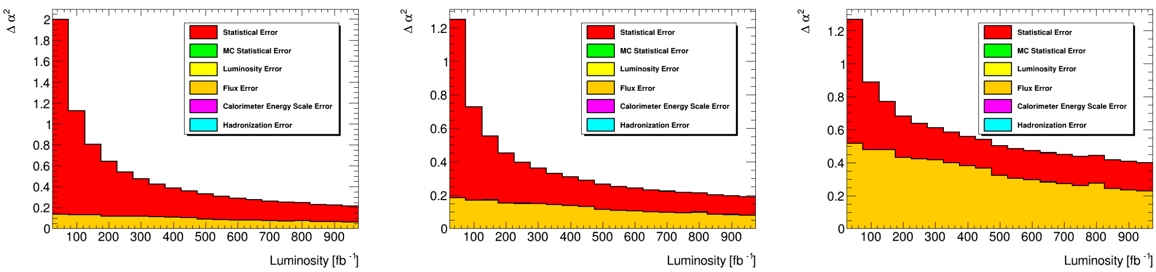

(a) bin 0: [0,800] GeV (b) bin 1: [800,1300] GeV (c) bin 2: [1300,5150] GeV

Figure 16: Square of the α uncertainty of each bin with the muon detector. Stacked. The calorimeter uncertainty and Hadronization uncertainty are in the legend, but we don't calculate them.

3.9 Discussion

3.9.1 Significanceof the detection

The significance becomes 5 σ at about 500 fb^{-1}, whether there is a muon detector or not. We assume some systematic uncertainties are negligible, so these results are not certain. However, I think we can say we can detect the CCν_e event at Run4 even if there is no additional detector.
However, We can't see the big difference between them. it is strange from the number of the background difference. We have to understand why this result occurred. Figure 17 shows the flux uncertainty of background events.

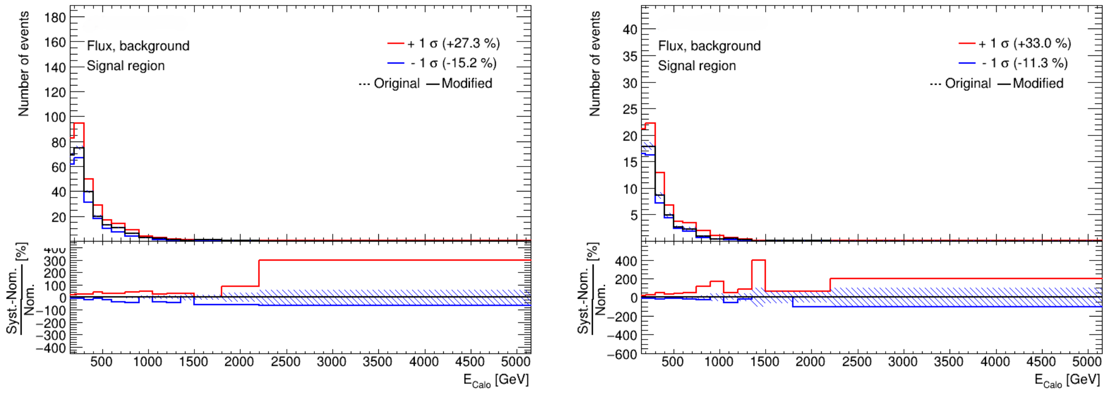

(a) without the muon detector

(b) with the muon detector

Figure 17: Distribution of background events. The uncertainty means only flux uncertainty of background events. The luminosity is set to 350 fb^{-1}

The uncertainty ratio to the events is almost the same. So, when there is a norm factor of background events, The effect of systematic uncertainty except for shape difference is the same. That's because the difference of the number of background is absorbed by the norm factor, and there is no constraint term of the background norm factor.
So, the difference between the result with the muon detector and one without the muon detector is the effect of the number of events at each bin and the shape difference. The effect of the number of events at each bin is defined by Poisson distribution, so the relative error decreases as the luminosity becomes big.The difference of significance follows this tendency. Figure 18 shows the result of the Likelihood ratio scan. The logged likelihood's shape looks different with or without systematic uncertainty.

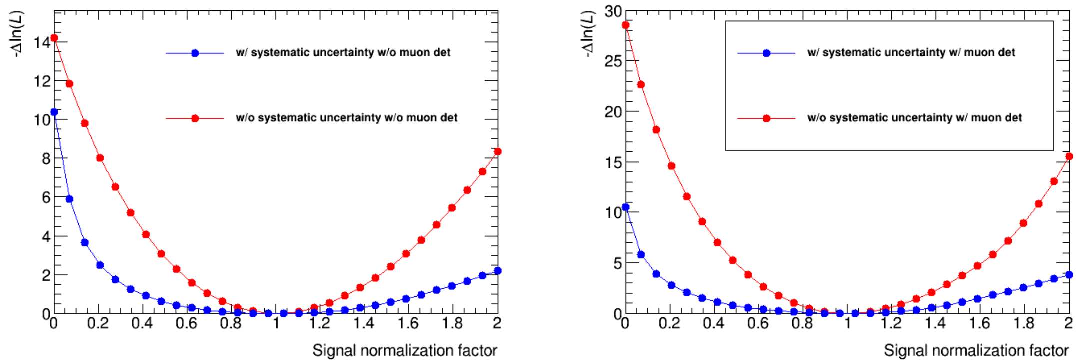

(a) without the muon detector (b) with the muon detector

Figure 18: The result of logged Likelihood ratio scan. The luminosity is set to 350 fb^{-1}

To validate the effect of ν_{bkg}, I check the significance without ν_{bkg}. Figure 19 shows the result.

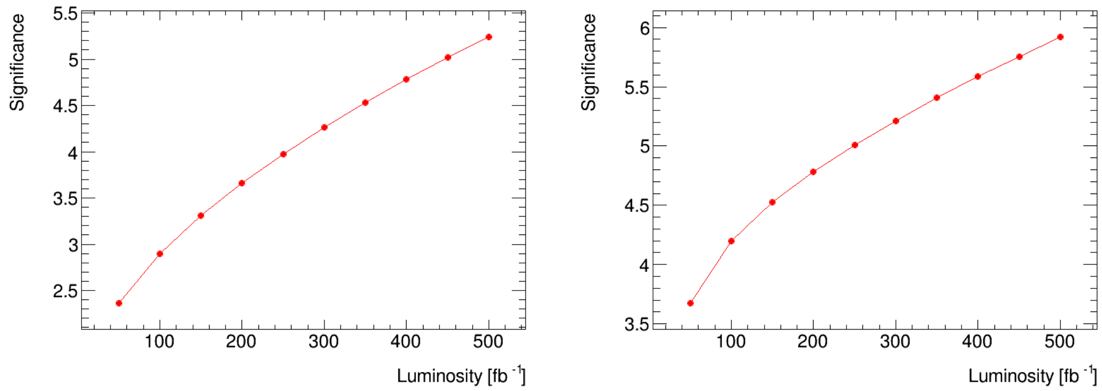

(a) without the muon detector (b) with the muon detector

Figure 19: Growth curve of the significance without ν_{bkg}.

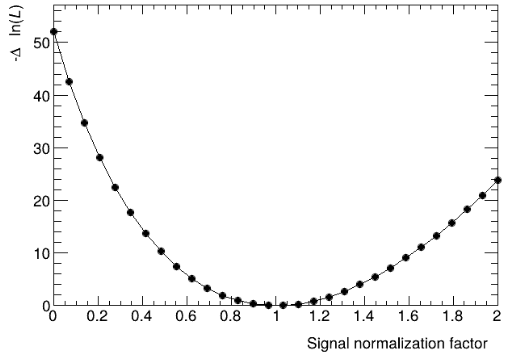

(a) without the muon detector and without systematic uncertainty

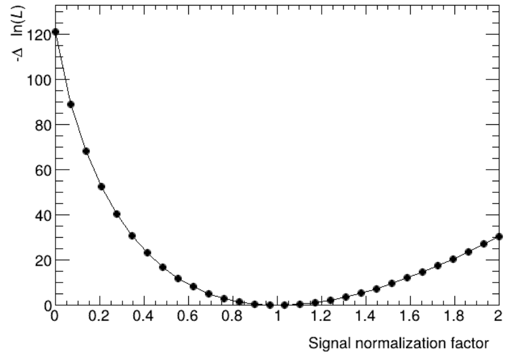

(b) with the muon detector and without systematic uncertainty

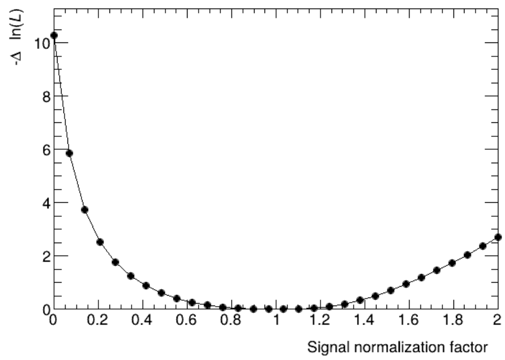

(c) without the muon detector and with systematic uncertainty

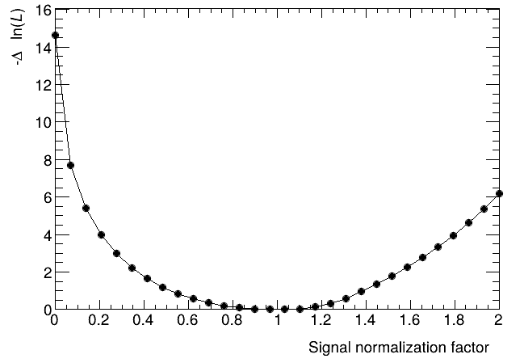

(d) with the muon detector and with systematic uncertainty

Figure 20: The result of logged Likelihood ratio scan without ν_{bkg}. The luminosity is set to 350 fb^{-1}

The significance of the result with the muon detector becomes bigger than before. However, the significance of the result without the muon detector become big only at low luminosity. So, when considering the likelihood that the number of the signal events is bigger than background, we shouldn't use the background norm factor. To evaluate the effect of the muon detector to the significance of the detection, we should compare the result without ν_{bkg}.[6] Then, the significance becomes 5.0σ at about 250 fb^{-1} and this is smaller than 450 fb^{-1}.

3.9.2 Uncertainty of α parameter: cross-section measurement

In Figure 13, the uncertainty decreases as the luminosity becomes big. However, the uncertainty is In Figure 16, you can see the statistical uncertainty decrease as the luminosity becomes big, but Flux uncertainty is not so.
This causes the invert the hierarchy of the α uncertainty at each bin and saturation of uncertainty of bin3.

[6] When evaluating the effect of the muon detector to the uncertainty of alpha parameter, there is no need to reject ν_{bkg}. That's because when evaluating the uncertainty we fit $\nu_{bkg} = 1$. To consider further, we have to select the likelihood function model by Information Criterion(AIC,BIC).

However, the average of the uncertainty is about 75 % at 500 fb^{-1}. So, I conclude we can measure the cross-section with 75 % uncertainty at 500 fb^{-1}.
If there is the muon detector, the systematic uncertainty and statistical uncertainty become smaller than without the muon detector. We can measure the cross-section with about 65 % uncertainty at 500 fb^{-1}. If there is 1 ab^{-1}, we can measure about 55 % uncertainty.

3.9.3 Optimization

The uncertainty in bin 3 is saturated because of the flux systematic uncertainty in the bin 3 range. The systematic uncertainty of the flux model becomes small as the bin range is small. However, The statical uncertainty becomes big as the bin range is small.
So we should optimize the binning of E_{truth} to reduce the total uncertainty at target luminosity.
Also, E_{calo} binning should be optimized because significance becomes big as the number of bins increases.
So, we have to optimize the parameters of this likelihood method and changeable selection as follows:

1. Threshold of E_{calo}:
   As I said before, this threshold should be optimized to reduce the background from neutral hadrons. Also, the significance can be roughly estimated by the number of signals per square root of the number of background $\frac{n_{sig}}{\sqrt{n_{bkg}}}$. Figure 21 show the dependence of the $\frac{n_{sig}}{\sqrt{n_{bkg}}}$ on the threshold.
   You can see $\frac{n_{sig}}{\sqrt{n_{bkg}}}$ has a highest value at about 300 GeV. So, setting the threshold as 300 GeV is optimal if the binning is optimal.

2. bin of E_{calo}:
   Normally, the number of bins should be big. However, the statistical uncertainty and MC statistical uncertainty become big if the statistics are too small.

3. Cut of the charge of pre-shower scintillators:
   This selection hasn't been mentioned. The charge of the pre-shower scintillator gives us the information where interaction occurs and E_{truth}. So we should optimize the cut of preshower value.
   Or, we can use this value for neutral hadron background estimation.

4. bin of E_{truth}(only for measuring the cross-section part):
   The binning of E_{truth} should be done by the physics motivation. However, as I said before, the statistical uncertainty and Flux uncertainty depend on binning, so we should optimize the binning of E_{truth} to reduce the total uncertainty at target luminosity.
   Roughly I investigate at 500 fb^{-1}, 3 bins look good, the statistical effect is bigger than the systematic effect at 6 bins

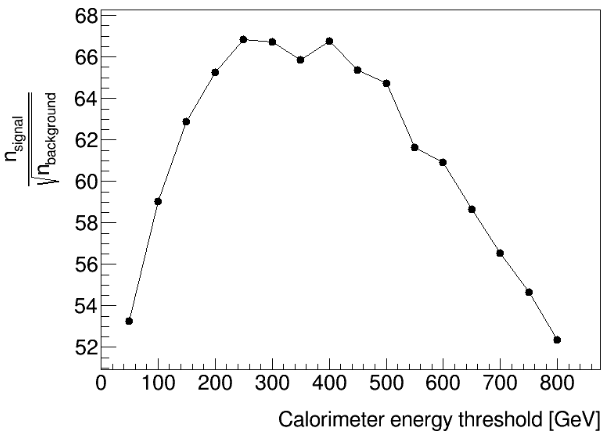

Figure 21: Dependence of the $\frac{n_{sig}}{\sqrt{n_{bkg}}}$ on the calorimeter energy threshold at 10 ab^{-1}

And not only these optimizations, but to evaluate the most effective Likelihood function, we have to optimize the likelihood function using Information Criteria (AIC, BIC, etc).

3.10 Selecting the most suitable flux model

To select the most suitable flux model, we cannot use LRT(Likelihood ratio test).
Because the flux models and their generators aren't nested and the number of parameters is the same.
So, to evaluate, only we can do is comparing the NNL. So we have to set the likelihood. However, to evaluate the flux model, we shouldn't set the norm factor because the difference between models is not the shape but the scale.
So, I modify the likelihood as follows:

$$L(\boldsymbol{n_{data}}|\boldsymbol{\nu_{sys}},\boldsymbol{\gamma}) = \prod_{i}^{N} \left[\mathrm{Pois}(n^i_{\mathrm{data}}|n_i^{exp}) \times \mathrm{Pois}(m_i|\gamma_i m_i)\right] \tag{6}$$

$$n_i^{exp} = \gamma_i \prod_{sys} [\eta_{sys,i}(\nu_{sys})] \times n_i^{MC} \tag{7}$$

, where we use n_i^{MC} is the scaled number of both signal and background events at i bin.[7]
Systematic uncertainty is as follows:

1. Neutrino cross-section uncertainty:
   cross-section systematic uncertainty needs to be considered. As I said before the uncertainty of the generator is less than 6%[7]. Ideally, we should use the model difference between generators as the uncertainty, but it is hard to do the MC simulation for each model. So, now we set the systematic uncertainty as 6 % everywhere.

2. Luminosity uncertainty: same as Section 3.6.

[7]Now, I use pyhf for convenience. However, pyhf doesn't follow Beeston-Barlow methods for MC statistical uncertainty. so I use "shapeSys" and a relative error as input.https://github.com/scikit-hep/pyhf/discussions/1867

3. The calorimeter energy scale: same as Section 3.6.
4. The Number of Cluster in Tracker station 3: same as Section 3.6.
5. Hadronization in MC simulation: same as Section 3.6.
6. (Reality of structure in the MC simulation): same as Section 3.6.

.
Evaluating the possibility of Selecting the most suitable flux model is done as follows.

1. Using middle model:(EPOS + Monash), make the middle Asimov dataset.
2. Making the likelihood of each model
3. Fitting the likelihood of each model to the middle Asimov dataset, and get the NNL.

However, with the MC statistical uncertainty, the likelihood fit is not stable, so I neglect the MC statistical uncertainty in this section.
Binning is set to as follows:

$$\begin{aligned}&\text{binning of } E_{calo} \text{ [GeV]} =\\&(20, 40, 60, 80, 100, 120, 140, 160, 200, 300,\\&400, 500, 600, 750, 900, 1050, 1200, 1350, 1500, 1800, 2200, 5150)\end{aligned}$$

Figure 22 shows the result. There are no common criteria for model rejection because this NNL doesn't follow the $\chi^2(1)$ distribution. So, we can't do the statistical test. So, now we can't say what luminosity needed to reject each model. However, for my information, I plot the line: NNL = 10.

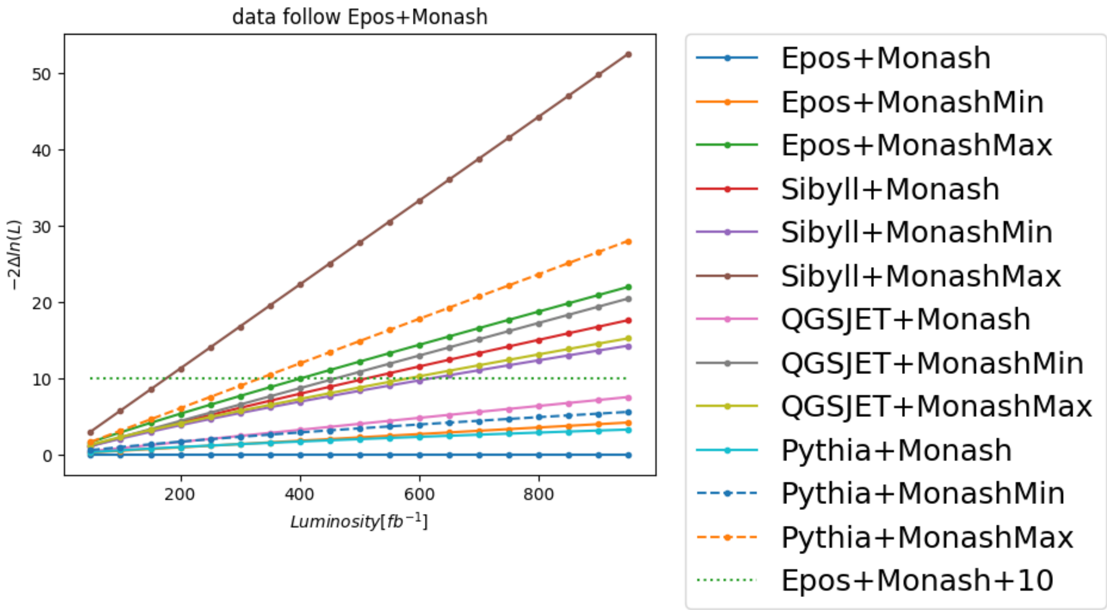

Figure 22: Logged likelihood growth plot. The target of the fitting is Asimov data following the "EPOS + Monash" model. The y-axis is the difference in logged likelihood between the model and the "EPOS + Monash" model. MC statistical uncertainty is neglected. The binning of the calorimeter energy is not optimized. Be careful that the difference in logged likelihood does not follow χ^2 distribution.

4 Conclusion

In this report, I have presented an analysis for detecting ν_e and measuring its cross-section using the FASER detector. The statistical analysis indicated that, while the current significance for detecting ν_e is not reached to 3σ, we will able to detect ν_e using this method by the end of Run-4. The significance becomes 5σ at about 450 fb^{-1} without the muon detector, at about 250 fb^{-1} with the muon detector behind the calorimeter with sufficient materials. The uncertainty of cross-section becomes under 70 % at 500 fb^{-1}. Additionally, the inclusion of the muon detector behind the calorimeter could reduce the uncertainty of measuring about 10 %.
Future work will focus on developing ways to evaluate the systematic uncertainty not considered now and optimization of likelihood fit and selection. After the preliminary part of this analysis ends, the data will open and the result will published. I hope it goes well.

5 acknowledgement

Special thanks to my supervisors, Tomohiro Inada and Susanne Kühn, for all kinds of help. And, I would like to thank Tomohiro Inada for the discussion of my study and a lot of advice.
I am also thankful to the CERN summer student team, my home institution supervisor,

colleagues at CERN, and my family. Finally, my stay at CERN as a summer student is supported by the KEK International and inter-institution Network for Accelerator Science to Next Generation(IINAS-NX).

References

[1] Search for Axion-like Particles in Photonic Final States with the FASER Detector at the LHC. Technical report, CERN, Geneva, 2024.

[2] Roshan Mammen Abraham, John Anders, Claire Antel, Akitaka Ariga, Tomoko Ariga, Jeremy Atkinson, Florian U. Bernlochner, Tobias Boeckh, Jamie Boyd, Lydia Brenner, Angela Burger, Franck Cadoux, Roberto Cardella, David W. Casper, Charlotte Cavanagh, Xin Chen, Andrea Coccaro, Stephane Débieux, Monica D'Onofrio, Ansh Desai, Sergey Dmitrievsky, Sinead Eley, Yannick Favre, Deion Fellers, Jonathan L. Feng, Carlo Alberto Fenoglio, Didier Ferrere, Max Fieg, Wissal Filali, Haruhi Fujimori, Ali Garabaglu, Stephen Gibson, Sergio Gonzalez-Sevilla, Yuri Gornushkin, Carl Gwilliam, Daiki Hayakawa, Shih-Chieh Hsu, Zhen Hu, Giuseppe Iacobucci, Tomohiro Inada, Luca Iodice, Sune Jakobsen, Hans Joos, Enrique Kajomovitz, Takumi Kanai, Hiroaki Kawahara, Alex Keyken, Felix Kling, Daniela Köck, Pantelis Kontaxakis, Umut Kose, Rafaella Kotitsa, Susanne Kuehn, Thanushan Kugathasan, Helena Lefebvre, Lorne Levinson, Ke Li, Jinfeng Liu, Margaret S. Lutz, Jack MacDonald, Chiara Magliocca, Fulvio Martinelli, Lawson McCoy, Josh McFayden, Andrea Pizarro Medina, Matteo Milanesio, Théo Moretti, Magdalena Munker, Mitsuhiro Nakamura, Toshiyuki Nakano, Friedemann Neuhaus, Laurie Nevay, Motoya Nonaka, Kazuaki Okui, Ken Ohashi, Hidetoshi Otono, Hao Pang, Lorenzo Paolozzi, Brian Petersen, Markus Prim, Michaela Queitsch-Maitland, Hiroki Rokujo, Elisa Ruiz-Choliz, André Rubbia, Jorge Sabater-Iglesias, Osamu Sato, Paola Scampoli, Kristof Schmieden, Matthias Schott, Anna Sfyrla, Mansoora Shamim, Savannah Shively, Yosuke Takubo, Noshin Tarannum, Ondrej Theiner, Eric Torrence, Svetlana Vasina, Benedikt Vormwald, Di Wang, Yuxiao Wang, Eli Welch, Samuel Zahorec, Stefano Zambito, and Shunliang Zhang. First measurement of ν_e and ν_μ interaction cross sections at the lhc with faser's emulsion detector. *Phys. Rev. Lett.*, 133:021802, Jul 2024.

[3] Henso Abreu, John Anders, Claire Antel, Akitaka Ariga, Tomoko Ariga, Jeremy Atkinson, Florian U. Bernlochner, Tobias Blesgen, Tobias Boeckh, Jamie Boyd, Lydia Brenner, Franck Cadoux, David W. Casper, Charlotte Cavanagh, Xin Chen, Andrea Coccaro, Ansh Desai, Sergey Dmitrievsky, Monica D'Onofrio, Yannick Favre, Deion Fellers, Jonathan L. Feng, Carlo Alberto Fenoglio, Didier Ferrere, Stephen Gibson, Sergio Gonzalez-Sevilla, Yuri Gornushkin, Carl Gwilliam, Daiki Hayakawa, Shih-Chieh Hsu, Zhen Hu, Giuseppe Iacobucci, Tomohiro Inada, Sune Jakobsen, Hans Joos, Enrique Kajomovitz, Hiroaki Kawahara, Alex Keyken, Felix Kling, Daniela Köck, Umut Kose, Rafaella Kotitsa, Susanne Kuehn, Helena Lefebvre, Lorne Levinson, Ke Li, Jinfeng Liu, Jack MacDonald, Chiara Magliocca, Fulvio Martinelli, Josh McFayden, Matteo Milanesio, Dimitar Mladenov, Théo Moretti, Magdalena Munker, Mitsuhiro Nakamura, Toshiyuki Nakano, Marzio Nessi, Friedemann Neuhaus, Laurie Nevay, Hidetoshi Otono,

Hao Pang, Lorenzo Paolozzi, Brian Petersen, Francesco Pietropaolo, Markus Prim, Michaela Queitsch-Maitland, Filippo Resnati, Hiroki Rokujo, Elisa Ruiz-Choliz, Jorge Sabater-Iglesias, Osamu Sato, Paola Scampoli, Kristof Schmieden, Matthias Schott, Anna Sfyrla, Savannah Shively, Yosuke Takubo, Noshin Tarannum, Ondrej Theiner, Eric Torrence, Serhan Tufanli, Svetlana Vasina, Benedikt Vormwald, Di Wang, Eli Welch, and Stefano Zambito. First direct observation of collider neutrinos with faser at the lhc. *Phys. Rev. Lett.*, 131:031801, Jul 2023.

[4] Henso Abreu, John Anders, Claire Antel, Akitaka Ariga, Tomoko Ariga, Jeremy Atkinson, Florian U. Bernlochner, Tobias Boeckh, Jamie Boyd, Lydia Brenner, Franck Cadoux, David W. Casper, Charlotte Cavanagh, Xin Chen, Andrea Coccaro, Monica D'Onofrio, Ansh Desai, Sergey Dmitrievsky, Candan Dozen, Yannick Favre, Deion Fellers, Jonathan L. Feng, Carlo Alberto Fenoglio, Didier Ferrere, Iftah Galon, Stephen Gibson, Sergio Gonzalez-Sevilla, Yuri Gornushkin, Carl Gwilliam, Daiki Hayakawa, Shih-Chieh Hsu, Zhen Hu, Giuseppe Iacobucci, Tomohiro Inada, Sune Jakobsen, Hans Joos, Enrique Kajomovitz, Hiroaki Kawahara, Alex Keyken, Felix Kling, Daniela Köck, Umut Kose, Rafaella Kotitsa, Susanne Kuehn, Helena Lefebvre, Lorne Levinson, Ke Li, Jinfeng Liu, Jack MacDonald, Chiara Magliocca, Fulvio Martinelli, Josh McFayden, Sam Meehan, Matteo Milanesio, Théo Moretti, Magdalena Munker, Mitsuhiro Nakamura, Toshiyuki Nakano, Friedemann Neuhaus, Laurie Nevay, Ken Ohashi, Hidetoshi Otono, Hao Pang, Lorenzo Paolozzi, Brian Petersen, Markus Prim, Michaela Queitsch-Maitland, Hiroki Rokujo, Elisa Ruiz-Choliz, Jorge Sabater-Iglesias, Jakob Salfeld-Nebgen, Osamu Sato, Paola Scampoli, Kristof Schmieden, Matthias Schott, Anna Sfyrla, Savannah Shively, Yosuke Takubo, Noshin Tarannum, Ondrej Theiner, Eric Torrence, Sebastian Trojanowski, Svetlana Vasina, Benedikt Vormwald, Di Wang, Eli Welch, Samuel Zahorec, and Stefano Zambito. Search for dark photons with the faser detector at the lhc. *Physics Letters B*, 848:138378, 2024.

[5] Henso Abreu, Elham Amin Mansour, Claire Antel, Akitaka Ariga, Tomoko Ariga, Florian Bernlochner, Tobias Boeckh, Jamie Boyd, Lydia Brenner, Franck Cadoux, David W. Casper, Charlotte Cavanagh, Xin Chen, Andrea Coccaro, Olivier Crespo-Lopez, Stéphane Débieux, Sergey Dmitrievsky, Monica D'Onofrio, Liam Dougherty, Candan Dozen, Abdallah Ezzat, Yannick Favre, Deion Fellers, Jonathan L. Feng, Didier Ferrere, Edward Karl Galantay, Jonathan Gall, Enrico Gamberini, Stephen Gibson, Sergio Gonzalez-Sevilla, Yuri Gornushkin, Carl Gwilliam, Daiki Hayakawa, Shih-Chieh Hsu, Zhen Hu, Giuseppe Iacobucci, Tomohiro Inada, Sune Jakobsen, Eliott Johnson, Enrique Kajomovitz, Hiroaki Kawahara, Felix Kling, Umut Kose, Rafaella Kotitsa, Jesse Krusse, Susanne Kuehn, Helena Lefebvre, Lorne Levinson, Ke Li, Jinfeng Liu, Chiara Magliocca, Fulvio Martinelli, Josh McFayden, Sam Meehan, Matteo Milanesio, Manato Miura, Dimitar Mladenov, Théo Moretti, Magdalena Munker, Mitsuhiro Nakamura, Toshiyuki Nakano, Marzio Nessi, Friedemann Neuhaus, Laurie Nevay, John Osborne, Hidetoshi Otono, Carlo Pandini, Hao Pang, Lorenzo Paolozzi, Brian Petersen, Francesco Pietropaolo, Markus Prim, Michaela Queitsch-Maitland, Filippo Resnati, Chiara Rizzi, Hiroki Rokujo, Elisa Ruiz-Choliz, Jakob Salfeld-Nebgen, Francisco Sanchez Galan, Osamu Sato, Paola Scampoli, Kristof Schmieden, Matthias Schott, Anna Sfyrla, Savannah Shively, Roland Sipos, John Spencer, Yosuke Takubo, Noshin Taran-

num, Ondrej Theiner, Pierre Thonet, Eric Torrence, Serhan Tufanli, Svetlana Vasina, Camille Vendeuvre, Benedikt Vormwald, Di Wang, Stefano Zambito, and Gang Zhang. The faser detector. *Journal of Instrumentation*, 19(05):P05066, May 2024.

[6] Konstantia Balasi, Christos Markou, K. Tzamarioudaki, P. Rapidis, Evangelia Drakopoulou, K. Pikounis, and C. Begatelas. The response of an autonomous underwater telescope to high energy neutrinos for the observation of gamma-ray bursts (grbs). *HNPS Proceedings*, 22:88, 03 2019.

[7] FASER Collaboration, Roshan Mammen Abraham, John Anders, Claire Antel, Akitaka Ariga, Tomoko Ariga, Jeremy Atkinson, Florian U. Bernlochner, Tobias Boeckh, Jamie Boyd, Lydia Brenner, Angela Burger, Franck Cadoux, Roberto Cardella, David W. Casper, Charlotte Cavanagh, Xin Chen, Andrea Coccaro, Stephane Débieux, Monica D'Onofrio, Ansh Desai, Sergey Dmitrievsky, Sinead Eley, Yannick Favre, Deion Fellers, Jonathan L. Feng, Carlo Alberto Fenoglio, Didier Ferrere, Max Fieg, Wissal Filali, Stephen Gibson, Sergio Gonzalez-Sevilla, Yuri Gornushkin, Carl Gwilliam, Daiki Hayakawa, Shih-Chieh Hsu, Zhen Hu, Giuseppe Iacobucci, Tomohiro Inada, Luca Iodice, Sune Jakobsen, Hans Joos, Enrique Kajomovitz, Hiroaki Kawahara, Alex Keyken, Felix Kling, Daniela Köck, Pantelis Kontaxakis, Umut Kose, Rafaella Kotitsa, Susanne Kuehn, Thanushan Kugathasan, Helena Lefebvre, Lorne Levinson, Ke Li, Jinfeng Liu, Margaret S. Lutz, Jack MacDonald, Chiara Magliocca, Fulvio Martinelli, Lawson McCoy, Josh McFayden, Andrea Pizarro Medina, Matteo Milanesio, Théo Moretti, Magdalena Munker, Mitsuhiro Nakamura, Toshiyuki Nakano, Friedemann Neuhaus, Laurie Nevay, Ken Ohashi, Hidetoshi Otono, Hao Pang, Lorenzo Paolozzi, Brian Petersen, Markus Prim, Michaela Queitsch-Maitland, Hiroki Rokujo, Elisa Ruiz-Choliz, André Rubbia, Jorge Sabater-Iglesias, Osamu Sato, Paola Scampoli, Kristof Schmieden, Matthias Schott, Anna Sfyrla, Mansoora Shamim, Savannah Shively, Yosuke Takubo, Noshin Tarannum, Ondrej Theiner, Eric Torrence, Svetlana Vasina, Benedikt Vormwald, Di Wang, Yuxiao Wang, Eli Welch, Samuel Zahorec, Stefano Zambito, and Shunliang Zhang. Neutrino rate predictions for faser, 2024.

[8] Kyle Cranmer, George Lewis, Lorenzo Moneta, Akira Shibata, and Wouter Verkerke. HistFactory: A tool for creating statistical models for use with RooFit and RooStats. Technical report, New York U., New York, 2012.

[9] Jonathan L. Feng, Iftah Galon, Felix Kling, and Sebastian Trojanowski. Forward search experiment at the lhc. *Phys. Rev. D*, 97:035001, Feb 2018.

[10] Markus Zerlauth and Oliver Bruning. Status and prospects of the HL-LHC project. *PoS*, EPS-HEP2023:615, 2024.